# Long-term trend of ozone pollution in China during 2014-2020: distinct seasonal and spatial characteristics **and ozone sensitivity**

Wenjie Wang[1], David D. Parrish[2], Siwen Wang[1], Fengxia Bao[1], Ruijing Ni[3], Xin Li[4], Suding Yang[4], Hongli Wang[5], Yafang Cheng[3], Hang Su[1]*

[1] Multiphase Chemistry Department, Max Planck Institute for Chemistry, Mainz, 55128, Germany.

[2] David. D. Parrish, LLC, Boulder, CO, 80303, USA.

[3] Minerva Research Group, Max Planck Institute for Chemistry, Mainz 55128, Germany.

[4] State Key Joint Laboratory of Environmental Simulation and Pollution Control, College of Environmental Sciences and Engineering, Peking University, Beijing, 100871, China.

[5] State Environmental Protection Key Laboratory of Formation and Prevention of Urban Air Pollution Complex, Shanghai Academy of Environmental Sciences, Shanghai 200233, China.

* Corresponding author.

Address: Multiphase Chemistry Department, Max Planck Institute for Chemistry, Mainz 55128, Germany.

Email: h.su@mpic.de

**Abstract:** In the past decade, ozone ($O_3$) pollution has become a severe environmental problem in major cities in China. Here, based on available observational records, we investigated the long-term trend of ozone pollution in China during 2014–2020. Ozone concentrations were slightly higher in urban areas than in non-urban areas. During these seven years, the highest ozone concentrations primarily occurred in summer in northern China, and in autumn or spring in southern China. Although ozone precursors, including nitrogen oxides ($NO_X$) and carbon monoxide (CO), continuously decreased, ozone concentrations generally increased throughout the seven years with a slower increasing rate after 2017. The long-term trend of ozone concentrations differed across seasons; especially from 2019 to 2020 when ozone concentrations decreased in summer and increased in winter. To analyze the causes of this observed trend, a photochemical box model was used to investigate the change in ozone sensitivity regime in two representative cities – Beijing and Shanghai. Our model simulations suggest that the summertime ozone sensitivity regime in urban areas of China has changed from a VOC-limited regime to a transition regime during 2014–2020; by 2020, the urban photochemistry is in a transition regime in summer but in a VOC-limited regime in winter. This study helps to understand the distinct trends of ozone in China and provides insights into efficient future ozone control strategies in different regions and seasons.

## 1 Introduction

Tropospheric ozone ($O_3$) is an air pollutant that is detrimental to human health, vegetation and ecosystem productivity (Ainsworth et al., 2012;Mills et al., 2018;Monks et al., 2015;Fiore et al., 2009). The inhalation of ozone impairs the functioning of the human respiratory and cardiovascular systems through its reaction with the lining of the lung and other surfaces in the respiratory tract (Jindal, 2007). Ozone is also an important greenhouse gas that leads to positive radiative forcing (Stocker et al., 2014). A comprehensive characterization of the spatial (latitude, longitude and altitude) and temporal distribution of tropospheric ozone is critical to our understanding of these issues. Here we summarize this distribution over China from the available observational records to the extent possible.

China has undergone rapid economic development, leading to higher demand for energy, and greater usage of fossil fuels during the past several decades. As a result, high anthropogenic emissions to the atmosphere have produced severe ozone pollution in urban areas of China, where daily maximum 8-hour average (MDA8) ozone concentrations often exceed the standard of 80 ppb (Li et al., 2014;Li et al., 2019a;Zhang et al., 2014;Lu et al., 2018). In contrast to the generally decreasing ozone levels in the United States and Europe, available surface ozone observations have widely shown significant upward trends in China since 1990 in rural areas (Wang et al., 2009;Ma et al., 2016;Sun et al., 2016;Xu et al., 2020), urban areas (Li et al., 2019a;Wang et al., 2020;Zhang et al., 2014;Lu et al., 2018), and over regional scales (Verstraeten et al., 2015;Xu and Lin, 2011). Measured ozone trends in previous studies are summarized in **Table 1**. For direct comparison of these results reported in different units, we have included estimated trends in units of % $yr^{-1}$ for all studies. Xu and Lin (2011) and Verstraeten et al. (2015) have reported that tropospheric ozone concentrations increased in summer during 1979–2005 in the North China Plain and 2005–2010 in Eastern China at a rate of 1.1% and 3.0% $yr^{-1}$, respectively, based on satellite measurements. Urban ozone concentrations increased significantly in Beijing,

91  Shanghai, Hongkong, Sichuan Basin and other cities during the past one to two

92  decades at rates of 2.0 to 6.7% yr$^{-1}$ (Gao et al., 2017;Cheng et al., 2016;Wang et al.,

93  2020;Chen et al., 2021b;Li et al., 2020;Lu et al., 2018). A significant increase in

94  ozone (+1.6% yr$^{-1}$) was detected at Shangdianzi, a rural site in the North China Plain

95  (Ma et al., 2016). A moderate increase was detected at the global background site

96  (Waliguan site) in western China (+0.44% yr$^{-1}$) (Xu et al., 2018;Xu et al., 2020). No

97  significant trend was detected at either the eastern coastal Changdao site (Wang et al.,

98  2020) or the Longfengshan site on the northeastern edge of China (Xu et al., 2020)..

99  In general, these studies show that ozone concentrations in China have risen in the

100 past three to four decades. As a result, China has become a global hot spot of ground-

101 level ozone pollution. The present annual mortality attributed to long-term ozone

102 exposure in China is estimated to be ~50,000 to 316,000 deaths (Liu et al.,

103 2018;Malley et al., 2017).

104     Global model simulations suggest that the average lifetime of ozone in the

105 troposphere is about 22 days (Stevenson et al., 2006;Young et al., 2013). In the free

106 troposphere at northern midlatitudes, where prevailing westerly winds dominate, the

107 net ozone lifetime is considerably longer, and is greater than the transport time around

108 the Earth (Trickl et al., 2011). Consequently, the increase in ozone in China not only

109 influenced domestic public health, but also influenced downwind countries (Brown-

110 Steiner and Hess, 2011;Lin et al., 2012) and thus increased global background ozone

111 concentrations. Several studies indicate that rising Asian emissions influenced

112 baseline ozone concentrations in America and Europe through the hemispheric

113 transmission of ozone and its precursors (Cooper et al., 2010;Verstraeten et al., 2015).

114 The baseline ozone concentrations at northern midlatitudes increased at an average

115 rate of ~ 0.60 ppb year$^{-1}$ from 1980 to 2000 (Parrish et al., 2020). Such an increase in

116 baseline ozone concentrations makes it more difficult to further reduce ozone in

117 America and Europe. Gaudel et al. (2020) reported that tropospheric ozone has

118 increased above 11 regions of the Northern Hemisphere since the mid-1990s.

119 Therefore, a detailed characterization of ozone pollution in China will aid

understanding of the variation in baseline ozone and guide the reduction of ozone throughout northern midlatitudes.

Chinese government launched the Air Pollution Prevention and Control Action Plan in 2013–2017 and the Clean Air Action plan in 2018–2020 to reduce anthropogenic emissions (Cheng et al., 2019). In this case, ozone precursors decreased a lot while ozone pollution remained severe (Shao et al., 2021). Therefore, it is necessary to clearly understand the response of ozone to precursors' changes. The response of ozone to precursors' changes is primarily determined by the ozone precursor sensitivity. Wang et al. (2021) has analyzed the ozone precursor sensitivity using satellite observations of formaldehyde to $NO_2$. There are more other studies analyzing the ozone precursor sensitivity by using chemical transport models (Chen et al., 2021a;Kang et al., 2021;Li et al., 2019a). Comprehensive measurements of $O_3$ precursors (VOCs and $NO_X$) and meteorological factors (photolysis frequencies, temperature and humidity) help to better identify the ozone precursor sensitivity (Kleinman et al., 1997;Kleinman, 2005). In this study, with comprehensive measurement data constrained in the observation-based box model, the ozone sensitivity regimes can be better diagnosed (Wang et al., 2020) and become complimentary to early studies. The goal of this study is to elucidate the spatial distribution, seasonal variation and temporal trends of ozone as well as the ozone precursor sensitivity in China by using comprehensive surface observations. Our study will provide a better understanding of the response of ozone to emission reductions, and inform the development of control measures to effectively mitigate ozone in the future.

## 2 Method

### 2.1 Measurements

Hourly surface $O_3$, nitrogen dioxide ($NO_2$) and carbon monoxide (CO) concentrations during 2014–2020 were obtained from the public website of the China

Ministry of Ecology and Environment (MEE) (https://quotsoft.net/air/). The surface monitoring network covered 940 stations in summer 2014, and extended to 1669 stations by 2020 (~330 cities). The $O_3$ concentrations at 750 sites with continuous observations over these 7 years were analyzed. These measurements document the air quality in Chinese cities and have been analyzed in recent studies (Li et al., 2019a;Lu et al., 2018). Total solar radiation data in 2013 were acquired from the meteorological data set of fundamental meteorological elements of China national weather station (V3.0), but data after 2013 are unavailable.

The Tropospheric Assessment Report (Fleming et al., 2018) used the population density together with NOAA night-time lights to classify the urban and non-urban sites. Given that it is not easy to acquire the night-time light data in China, urban and non-urban sites are distinguished by population density in this study. Population density data were acquired from Gridded Population of the World (GPW), v4; https://sedac.ciesin.columbia.edu/data/set/gpw-v4-population-density-rev11. This is a dataset of the world population gridded at ~5 km resolution. According to the China Statistical Yearbook in 2018 (China Statistics Press, 2018), China's urban population density was 2500 people/km$^2$. In the following analysis, urban sites correspond to population density ≥2500 people/km$^2$, and non-urban sites correspond to population density <2500 people/km$^2$.

To reflect the breadth of different health-related indicators used globally, four metrics—AVGMDA8, 4MDA8, NDGT70, 3MMDA1—are used here to characterize ozone pollution levels. The definitions of these metrics are given in **Table 1**. AVGMDA8 represents the mean value of daily maximum 8 h average (MDA8) ozone concentrations, and 4MDA8 represents the annual 4th highest (MDA8) ozone concentrations; 3MMDA1 represents the annual maximum of the 3-month running mean of the daily maximum 1-hour (MDA1) ozone concentrations. Since these metrics are determined from different parts of the distribution of ozone concentrations, their spatial distribution and temporal variation may differ. We derived all metrics from the hourly measurements that were filtered by data quality control procedures following the Tropospheric Ozone Assessment Report (TOAR) data completeness

requirements and procedures (Lefohn et al., 2018). The calculations of AVGMDA8, 4MDA8, NDGT70 are based on MDA8 ozone concentrations. MDA8 ozone concentration is the maximum value of 8-hour running averages calculated from 0 h to 23 h local time. Note that if the data availability at a certain site is less than 60% (i.e., less than 5 hours for 8-hour averages or 15 hours for one day), the MDA8 value was considered missing. For the calculation of these metrics (AVGMDA8, 4MDA8, NDGT70), if less than 60% of MDA8 values are available (i.e., less than 220 MDA8values for a year or 55 MDA8 values for a season), the annual mean or seasonal mean values of the metrics at a certain site were considered missing. The calculation of 3MMDA1 was based on the daily maximum 1-hour (MDA1) ozone value. Similar to the MDA8 ozone value, if less than 60% of data are available (i.e. less than 15 hours for one day), the MDA1 value at a certain site was considered missing. For the calculation of 3MMDA1, if less than 60% of MDA1 values are available (i.e. less than 55 MDA1 values for three months and 220 MDA1 values for a year), the 3MMDA1 value at a certain site was considered missing.

Beijing and Shanghai are the two largest cities in China and have undergone severe ozone pollution in the past decade (Wang et al., 2020;Xu et al., 2019). Measurement data in Beijing and Shanghai were analyzed to show the variation characteristic of ozone sensitivity regimes. The data of $O_3$, $NO_2$ and CO were acquired from the public website of the China Ministry of Ecology and Environment (https://quotsoft.net/air/). VOCs, and meteorological factors (including temperature, relative humidity, photolysis frequencies and air pressure) were measured during 2014–2020 at two representative urban sites in Beijing and Shanghai: Peking University and Shanghai Academy of Environmental Sciences. Temporal trends and composition of VOCs at the two sites were considered to be representative across Beijing and Shanghai (Wang et al., 2010;Xu et al., 2011;Zhang et al., 2012). VOCs were measured using a commercial gas chromatography-mass spectrometer/flame ionization detector (GC-MS/FID) system coupled with a cryogen-free preconcentration device (Wang et al., 2014). The system contains two-channel sampling and GC column separation which is able to measure C2–C5 hydrocarbons

**2.2 Zero-dimension photochemical box model**

A zero-dimension photochemical box model was used to simulate the sensitivity
of ozone production and loss to its precursor concentrations. Compared with regional
3-D models, the box model has the advantage that it can be constrained by
comprehensive measurements to eliminate the uncertainty from emission inventories.
The box model includes MCM v.3.3.1 as the chemical mechanism. Hourly averages
of CO, $NO_2$, NO, $O_3$, $SO_2$, VOCs (56 species), formaldehyde, acetaldehyde,
photolysis frequencies, temperature, air pressure, and relative humidity were used as
model constraints. HONO was not measured, and thus was calculated according to the
concentration of $NO_2$ and the observed ratio of HONO to $NO_2$ in Beijing (Hendrick et
al., 2014). The model simulations were performed in a time-dependent mode with
spin-up of two days. For physical removal processes, a 24-h lifetime was assumed for
all simulated species, which approximately simulates the effects of dilution and
surface deposition. This modeling approach has been used previously (Wang et al.,
2019;Wang et al., 2020;Wang et al., 2021b).

$RO_2$, $HO_2$ and OH radicals were simulated by the box model to calculate the net
ozone production rate ($P(O_3)$) and ozone loss rate ($L(O_3)$)as shown in Equation (1)
and (2) as derived by Mihelcic et al. (2003).

$$P(O_3) = k_{HO_2+NO}[HO_2][NO] + \sum_i(k^i_{RO_2+NO}[RO_2^i][NO]) - k_{OH+NO_2}[OH][NO_2] -$$

$$L(O_3) \tag{1}$$

$$L(O_3) = (\theta j(O^1D) + k_{OH+O_3}[OH] + k_{HO_2+O_3}[HO_2] +$$

$$\sum_j(k^j_{alkene+O_3}[alkene^j])[O_3] \tag{2}$$

where θ is the fraction of $O^1D$ from ozone photolysis that reacts with water vapour,

234    and i and j represent the number of species of $RO_2$ and alkenes, respectively.

## 3 Results and Discussion

**3.1 The spatial distribution and seasonal variation of ozone pollution**

237    **Figure 1** presents the spatial distributions of the mean values of four ozone
238    metrics (AVGMDA8, 4MDA8, NDGT70 and 3MMDA1) at non-urban and urban sites
239    in China during 2014–2020. The spatial distribution was similar between urban and
240    non-urban sites for all four metrics; for example, warm-season AVGMDA8 $O_3$
241    concentrations at 74% of urban sites and 67% of non-urban sites exceed the air quality
242    standard Grade 1 limit of 50 ppb. Hot spots of ozone pollution mainly occurred in the
243    more economically developed areas in northern, eastern and central China. At both
244    urban and non-urban sites, the highest regional average ozone concentrations occur in
245    the North China Plain with the average warm-season AVGMDA8 $O_3$ concentration of
246    66 ppb, significantly higher than the corresponding national average value of 54 ppb.
247    Although the solar radiation in the North China Plain is not the strongest across China
248    (Jiang et al., 2019), North China Plain has a large density of urban and industrial
249    activities. Previous studies denote that the North China Plain has the highest $NO_x$ and
250    VOCs emissions over China (Liu et al., 2016;Li et al., 2019b). This clearly indicates
251    that ozone pollution is closely related to anthropogenic activities. In addition, the high
252    $O_3$ concentration over the North China Plain is also related to the high temperature
253    extremes (Wang et al., 2021a).
254    The month in which the 3MMDA1 ozone concentration occurred is defined as
255    the middle month in the 3 months of 3MMDA1, which can indicate the season when
256    maximum ozone pollution occurred. As shown in **Fig. 2**, the month in which the
257    3MMDA1 ozone concentration occurred shows a significant spatial variation. In most
258    years, the 3MMDA1 ozone concentration in northern China (north of the Yangtze
259    River) occurred mainly in summer (June, July and August), whereas in southern
260    China (south of the Yangtze River), it occurred in autumn (September, October and

November) or spring (March, April, May). In northern China, sunlight intensity is highest in summer and photochemical production from anthropogenic and biogenic precursors maximizes. In southern China, the southwest monsoon prevails in summer leading to an inflow of marine air with low ozone concentrations and reduced photochemical ozone production due to more cloudy and rainy weather (Yin et al., 2019); thus in this region the highest ozone usually appears in autumn when sunlight intensity maximizes.

It is notable that the 3MMDA1 ozone concentration mainly occurred in spring in both Heilongjiang and Yunnan provinces, which are located in northeast and southwest China, respectively. This is consistent with a previous study reporting that Yunnan province and northeast China had peak $O_3$ in spring 2014–2017 (Yin et al., 2019). A springtime maximum was also found for the column $O_3$ in Yunnan retrieved from satellite data (Xiao and Jiang, 2013). The occurrence of maximum ozone concentrations in spring has been attributed to several factors, including 1) the peak occurrence of stratospheric intrusions, 2) photochemistry of precursors built up during winter, and 3) biomass-burning either as forest fires or for land clearance (Monks et al., 2015). Heilongjiang province is located in the northernmost part of China (43°26′N–53°33′N) with relatively low temperature and light intensity, and thus its photochemical production of ozone is weak all year round. We surmise that the springtime maxima of ozone in this province is due to the first two causes: the stratospheric intrusion of ozone in spring (Stohl et al., 2003), and ozone production in spring from accumulated precursors that were emitted from coal burning for heating during the wintertime. Yunnan province is located in a plateau area with average altitude of 2000 m; the elevated terrain of this province is more likely to be influenced by the descending free tropospheric air masses with high ozone concentrations from the stratospheric origin (Stohl et al., 2003;Cooper et al., 2012). Additionally, higher sunlight intensity in spring at this lower latitude province is also conducive to photochemical production of ozone.

We also compared the seasonal variations in MDA1 ozone concentrations in three typical Chinese city clusters, Beijing-Tianjin-Hebei (BTH), Yangtze River Delta

(YRD) and Pearl River Delta (PRD) (**Fig.3**). In each city cluster there is a distinct seasonal ozone pattern: a sharp unimodal distribution with a summer maximum in BTH, a broad distribution with a spring maximum in YRD, and a less distinct, unimodal distribution with an autumn maximum in PRD. Meteorological factors determine the different ozone distribution patterns; most importantly PRD and YRD received more precipitation in summer than BTH, and that PRD was especially affected by the inflow of marine air during the southwest monsoon. Furthermore, in PRD typhoons led to less cloud cover, and thus more solar radiation in autumn, which accelerated $O_3$ production (Qu et al., 2021). As shown in **Fig. 3**, the seasonal variations in ozone in the three city clusters are overall consistent with those of solar radiation in representative cities of the three city clusters (Beijing in BTH, Shanghai in YRD and Guangzhou in PRD). This result indicates that the local photochemistry driven by solar radiation plays a crucial role in ozone seasonal variations.

## 3.2 Temporal trend of ozone pollution

Ozone trends measured on regional scales, in urban areas, and at rural sites in previous studies are summarized in **Table 2**. For direct comparison of these results reported in different units, we have included estimated trends in units of % $yr^{-1}$ for all studies. Xu and Lin (2011) and Verstraeten et al. (2015) have reported that tropospheric ozone concentrations increased in summer during 1979–2005 in the North China Plain and 2005–2010 in Eastern China at a rate of 1.1% and 3.0% $yr^{-1}$, respectively, based on satellite measurements. Urban ozone concentrations increased significantly in Beijing, Shanghai, Hongkong, Sichuan Basin and other cities during the past one to two decades at rates of 2.0 to 6.7% $yr^{-1}$ (Gao et al., 2017;Cheng et al., 2016;Wang et al., 2020;Chen et al., 2021b;Li et al., 2020;Lu et al., 2018). A significant increase in ozone (+1.6% $yr^{-1}$) was detected at Shangdianzi, a rural site in the North China Plain (Ma et al., 2016). A moderate increase was detected at the global background site (Waliguan site) in western China (+0.44% $yr^{-1}$) (Xu et al., 2018;Xu et al., 2020). No significant trend was detected at either the eastern coastal

320 ~~Changdao site (Wang et al., 2020) or the Longfengshan site on the northeastern edge~~
321 ~~of China (Xu et al., 2020). The only significant decrease was reported at the Akedala~~
322 ~~site on the northwestern edge of China (-3.3% yr⁻¹) (Xu et al., 2020). In general, these~~
323 ~~studies show that ozone concentrations in China have risen in the past three to four~~
324 ~~decades.~~

325 **Figure 4** summarizes variations of four ozone metrics (warm season AVGMDA8,
326 4MDA8, 3MMDA1 and NDGT70) during 2014–2020 for Chinese urban and non-
327 urban sites. **Figure S1** presents the spatial distribution of warm season AVGMDA8
328 ozone concentrations at urban and non-urban sites for each year during 2014–2020.
329 The levels of these four metrics at urban sites were slightly higher than at non-urban
330 sites with difference less than 8% (**Fig. 4**). These results in China differ from those in
331 Europe and North America, where the mean levels of these metrics at urban sites were
332 slightly lower than those at non-urban sites (Fleming et al., 2018). From 2014 to 2020,
333 the trends of ozone were generally similar between urban and non-urban sites. The
334 four metrics all generally increased from 2014 to 2020 with the increasing rate getting
335 slower after 2017. Overall, the rapid increase in ozone concentrations in China has
336 either slowed or ended (depending upon metric) after 2017. During 2014-2017,
337 AVGMDA8 and NDGT70 increased at rates of 7.4% yr$^{-1}$ and 20% yr$^{-1}$ respectively.
338 4MDA8 and 3MMDA1, which characterize extremely high ozone levels, increased at
339 rates of 3.7% yr$^{-1}$ and 3.5% yr$^{-1}$ respectively. Obviously, the increasing rates of
340 4MDA8 and 3MMDA1 were significantly slower than those of AVGMDA8 and
341 NDGT70. In **Fig. 4**, the variations in the four metrics are fitted by quadratic functions.
342 The quadratic polynomial coefficients are all negative and statistically significant for
343 the four metrics, which is strong evidence that the increasing trend has slowed.

344 Because the trends of ozone are generally similar between urban and non-urban
345 sites (**Fig. 4**), the nationwide (including both urban and non-urban) AVGMDA8 was
346 used to analyze ozone trends for different seasons. **Figure 5** shows variations in
347 seasonal and annual AVGMDA8 during 2014–2020. For the national average,
348 AVGMDA8 was highest in summer, followed by spring, autumn, and winter. This
349 metric increased in all four seasons from 2014 to 2017, with the fastest increase in

spring (3.1 ppb yr$^{-1}$, r$^2$=0.94), followed by winter (2.9 ppb yr$^{-1}$, r$^2$=0.91), summer (2.0

ppb yr$^{-1}$, r$^2$=0.90) and autumn (1.2 ppb yr$^{-1}$, r$^2$=0.81). The annual average increased at

a rate of 2.0 ppb yr$^{-1}$ (r$^2$=0.95) from 2014 to 2017. The more rapid increase of ozone

concentration in spring than in summer resulted in a decrease in the gap between the

two seasons. This is consistent with a recent study reporting that ozone pollution in

the North China Plain extended to the spring season (Li et al., 2021). After 2017,

AVGMDA8 remained relatively stable in summer and spring, but still increased

significantly in autumn and winter. Compared with 2019, the seasonal average MDA8

ozone concentration decreased by 5.5 ppb in summer 2020, but increased by 5.1 ppb

in winter 2020. **Figure 6** illustrates the spatial patterns of the summer and winter

changes in seasonal average MDA8 O$_3$ from 2019 to 2020. In summer ozone

decreased significantly in most regions of China, with greater decreases in central

China and the North China Plain. In winter, ozone increased significantly throughout

China. The cause of these changes will be discussed in Section 3.3.

The trends of the ozone precursors, NO$_2$ and CO, were investigated based on the

observational data. As shown in **Fig. 7**, both NO$_2$ and CO decreased significantly

from 2014 to 2020 for both annual and seasonal averages. Notably, NO$_2$ decreased

faster after 2017 than before 2017. Both the MEIC inventory and OMI NO$_2$ data show

a decrease during 2013-2019 (Shah et al., 2020), which is consistent with our result.

The emission inventory suggests that VOCs emissions were stable during 2013-2019

in China (Li et al., 2019b;Zheng et al., 2021). In 2020 VOCs, CO and NO$_X$ emissions

decreased significantly in winter but only slightly in summer, compared to 2019

(Zheng et al., 2021), which is consistent with the changes of measured NO$_2$ and CO

(**Fig. 7**).

Figure 8 shows the trend of measured VOCs reactivity in Beijing and Shanghai

in summertime during 2014-2020. The VOCs reactivity is defined as the sum of all

VOCs concentrations multiplied by their respective reaction rate coefficients with OH,

as shown in Eq. 3. The VOCs reactivity is more related to ozone production rate than

VOCs concentrations (Zhang et al., 2014;Wang et al., 2020;Wang et al., 2021c). The

summertime VOCs reactivity decreased at a rate of -0.39 s$^{-1}$ (-7.5%) yr$^{-1}$ (r$^2$=0.56) in

Beijing and -0.46 s$^{-1}$ (-8.4%) yr$^{-1}$ (r$^2$=0.59) in Shanghai. It is notable that the trends of VOCs reactivity in Beijing and Shanghai are different from that of VOCs emissions across China.

$$VOCs\ reactivity = \sum_i^n k_{VOC_i}[VOC_i] \qquad\qquad (3)$$

$k_{VOC_i}$ represents the reaction rate coefficients between OH radicals and VOC species $i$. [VOC$_i$] is the concentration of VOC species $i$. n is the number of VOC species.

**3.3 The impact of photochemistry on ozone temporal trend**

Ozone concentrations are influenced by photochemical processes that depend on precursor concentrations and meteorological conditions. Changes in ozone precursor emissions, particularly VOC and NO$_X$, are the primary factors driving ozone trends in China. The relationship between O$_3$ and its precursor concentrations is generally nonlinear—a decrease in precursor concentrations does not necessarily result in a corresponding decrease in O$_3$ concentration. Differing responses of ozone production to VOC and NOx emission changes allow three ozone sensitivity regimes to be distinguished: VOC-limited, NOx-limited and transition regimes (Kleinman, 1994;Kleinman et al., 1997). In this section, based on comprehensive measurements in Beijing, the impact of photochemical regimes on the temporal trend of ozone in urban areas of China was discussed.

As discussed in Section 3.2, in summer when ozone pollution is most severe, ozone increased from 2014 to 2017, but remained relatively stable after 2017 (**Fig. 5**). To explore the impact of photochemical regimes on the temporal trend of ozone in summer, the zero-dimensional photochemical box model constrained by long-term measurements in Beijing and Shanghai was used to examine the variation in the sensitivity of ozone to precursor emissions. The ozone sensitivity regime was diagnosed by testing the response of P(O$_3$) as calculated from Equation (1) to the changes of VOCs and NO$_X$ concentrations (**Fig. 89**). The box model simulations suggest that in Beijing VOC reduction would significantly decrease ozone during all seven years, while NOx reduction would significantly increase ozone during 2014–

408  2017 but only slightly increase ozone in 2018 and slightly decrease ozone during

409  2019–2020. The 2014–2018 results are consistent with the VOC-limited regime in

410  which a reduction in VOCs is effective in mitigating ozone production, while a

411  reduction in $NO_X$ increases ozone production. The 2019–2020 results are consistent

412  with the transition regime in which reductions of either VOCs or $NO_X$ can decrease

413  ozone production. These results indicated that the summertime photochemical

414  environment in Beijing shifted from a VOC-limited regime to a transition regime. The

415  Shanghai simulations show similar behavior in terms of the shift in the photochemical

416  regime.

417  Previous 3-D model studies have reported results similar to our box model

418  simulation; urban areas in China were in the VOC-limited regime in the summer of

419  2013-2017, but in the transition regime after 2017 (Shao et al., 2021;Kang et al.,

420  2021;Li et al., 2019a). Tang et al. (2021) showed that ozone production in Beijing was

421  transitioning from VOC-sensitive to $NO_X$-sensitive over the 2013-2018 period. The

422  sharp decrease in $NO_X$ combined with a smaller change in VOCs in Shanghai has led

423  to a shift in the $O_3$ production from a VOC-limited regime to a $NO_X$-limited regime

424  over the past decade (Xu et al., 2019). In addition to model studies, satellite-observed

425  $HCHO/NO_2$ ratios also indicate that there is a shift in the  North China Plain, YRD

426  and PRD from the VOC-limited regime to the transitional regime, which is associated

427  with a rapid drop in anthropogenic NOx emissions from 2016 to 2019 (Wang et al.,

428  2021d). These studies agree that ozone sensitivity in summer in urban areas of China

429  has gradually changed from a VOC-limited regime to a transition or $NO_X$-limited

430  regime due to faster decreases in $NO_X$ emissions than in VOC emissions over the past

431  decade. Therefore, we surmise that the rapid increase of summertime ozone during

432  2013-2017 is due to the decrease in $NO_X$ under VOC-limited conditions, and that the

433  slowing of the summertime ozone increase after 2017 is due to decreased NOx

434  emissions and relatively stable VOC emissions under the transition regime conditions.

435  This finding lends more confidence to the effective reduction in summertime ozone

436  through continued reductions in VOC and $NO_X$ emissions.

437  Another issue is that compared to 2019, MDA8 ozone concentrations decreased

in summer but increased in winter in 2020 (**Fig. 5 and 6**) despite the decrease of $NO_X$, CO and VOCs (**Fig. 7**). Based on measurements in Beijing and Shanghai in 2019, the observation-based box model was used to examine the sensitivity of ozone to precursors in summer and winter. As shown in **Fig. 9 10**, in the summer of 2019, Beijing and Shanghai were in the transition regime, when reductions in VOCs and NOx both decreased the integrated ozone production rate. In winter it was in the VOC-limited regime, when reduction in VOCs decreased, but reduction in NOx increased, the ozone production rate. This result demonstrates that summer and winter had different ozone sensitivity characteristics in 2019. Based on WRF-Chem model simulations, Kang et al. (2021) also reported that ozone sensitivity entered the transition or $NO_X$-limited regime in summer 2020, but was still in the VOC-limited regime in winter 2020. In addition, the WRF-Chem model results by Le et al. (2020) indicate that the chemical regime was VOC-limited during the COVID-19 pandemic lockdown in winter 2020 in China and the decrease in $NO_X$ led to significant ozone increases. These studies are consistent with our simulation results in Beijing. The difference in ozone sensitivity regimes between winter and summer is likely to be a crucial cause of opposite ozone changes between winter and summer in 2020. Although ozone production rates and concentrations are much smaller in winter, ozone can influence particulate matter (PM) formation through increasing the atmospheric oxidizing capacity in this season (Le et al., 2020). Therefore, different ozone sensitivity regimes between winter and summer should be fully considered to effectively mitigate both ozone and PM in the two seasons.

Furthermore, the influence of meteorological factors on the ozone change from 2019 to 2020 was investigated. Table S1 shows the average values of primary meteorological factors including temperature, relative humidity, wind speed, wind direction, air pressure and photolysis frequency of $NO_2$ ($j(NO_2)$) in 2019 and 2020 in Beijing and Shanghai. Temperature increased in winter but decreased in summer from 2019 to 2020. Previous studies indicate that ozone concentrations show a positive correlation with temperature (He et al., 2017;Jacob and Winner, 2009). We surmise that the changes in temperature may partly contribute to the contrasting changes in

ozone concentrations between summer and winter from 2019 to 2020. Besides temperature, the significant changes in relative humidity may also influence the ozone change. $j(NO_2)$ maintained stable in both winter and summer from 2019 to 2020, indicating a minor effect of photolysis frequencies on ozone changes.

**3.4 Additional considerations**

There are several limitations of this study. One limitation is that the VOCs measurement data are only available in two megacities – Beijing and Shanghai. The trends of VOCs in Beijing and Shanghai cannot fully represent that in the whole country. As a result, the influence of the VOCs variation on the ozone trend across China is not completely elucidated. The diagnosis of ozone precursor sensitivity is also based on measurement data in the two megacities, which may not reflect the situation of the whole country. Another limitation of this study is that the photochemical box model is constrained by observations near the ground, hence may not accurately represent some aspects of the photochemistry throughout the boundary layer. The ozone precursor sensitivity in the upper layer of the boundary layer probably differs from that near ground under certain conditions due to varied VOCs and $NO_x$ levels and meteorological factors with height (Zhang et al., 2018;Sun et al., 2018). Therefore, to acquire a more broaden and comprehensive diagnosis of ozone precursor sensitivity, the measurement of VOCs in more cities and over the whole boundary layer is required in the future. Lastly, the transport effect of ozone is important in ozone pollution in China (Han et al., 2018;Shen et al., 2022;Yang et al., 2022). However, our study has not considered the transport effect which probably plays a crucial role in ozone trend and may also lead to uncertainties concerning the dignosis of ozone precursor sensitivities.

## 4 Conclusions

During the past decade, China has devoted substantial resources to improving the

environment. These efforts reduced atmospheric particulate matter loading, but ambient ozone levels increased (Shao et al., 2021). We present a detailed characterization of the spatial distribution and temporal trend of ozone over China based on nationwide hourly ozone observations, and find that:

(1) Maximum ozone concentrations primarily occur in summer in northern China, but in autumn or spring in southern China. Meteorological factors, especially solar radiation and the southwestern monsoon, play key roles in the regional contrast of the seasonal variations.

(2) Four ozone metrics (AVGMDA8, 4MDA8, NDGT70, 3MMDA1) increased from 2014 to 2017, and remained relatively stable after 2017. These metrics were generally higher at urban sites than at non-urban sites. The trend of ozone concentrations differed across seasons; especially from 2019 to 2020 when ozone concentrations decreased in summer and increased in winter.

(3) Simulations by an observationally constrained box model and previous 3-D model simulations agree that the ozone sensitivity in summer in urban areas of China gradually changed from the VOC-limited regime to a transition regime. This increases our confidence in the reduction of both VOC and NOx emissions as an effective approach to further reducing summertime ozone. Box model simulations also indicate that the urban photochemistry is still in the VOC-limited regime in winter in 2020.

Our study provides an improved understanding of the past and future response of ozone to emission reductions in China, and can inform control measures for effective future reductions of ozone.

## Data availability

The observational data and model code used in this study are available from corresponding authors upon request (h.su@mpic.de).

## Author contributions

HS and WW designed the research. WW and HS prepared the manuscript with contributions from other authors. WW performed data analysis with contributions from DP, SW, RN, FB and YC. HW, XL, SY collected data.

## Competing interests

The authors declare that they have no known competing financial interests or personal relationships that could have appeared to influence the work reported in this paper.

## Acknowledgements

This study is support by the Max Planck Society (MPG). Y.C. thanks the Minerva Program of MPG.
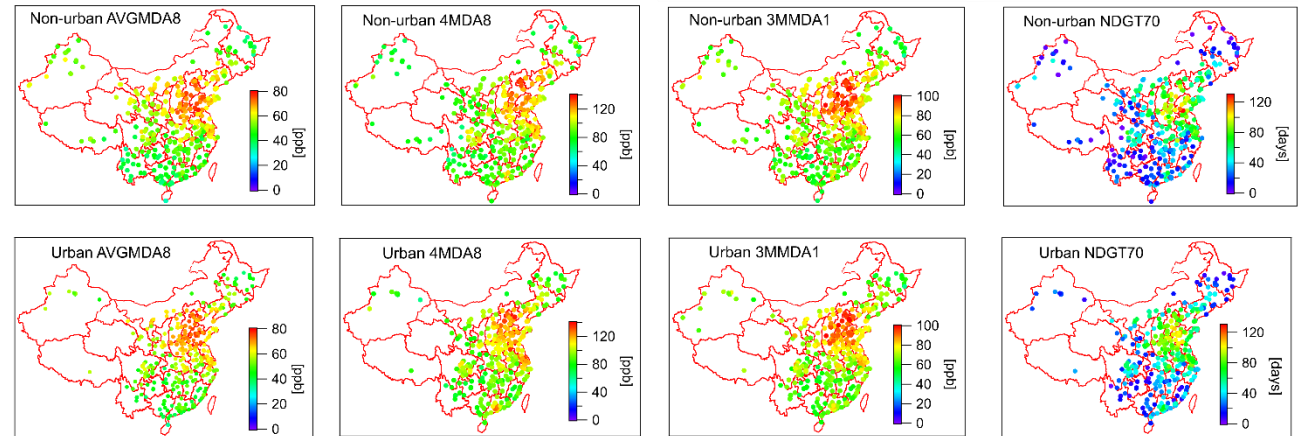
Figure 1. Spatial distribution of four ozone metrics (AVGMDA8, 4MDA8, 3MMDA1, NDGT70) at urban and non-urban sites averaged over 2014–2020. AVGMDA8 is the mean MDA8 $O_3$ in the warm season (April to September); other metrics are annual values.

562

563
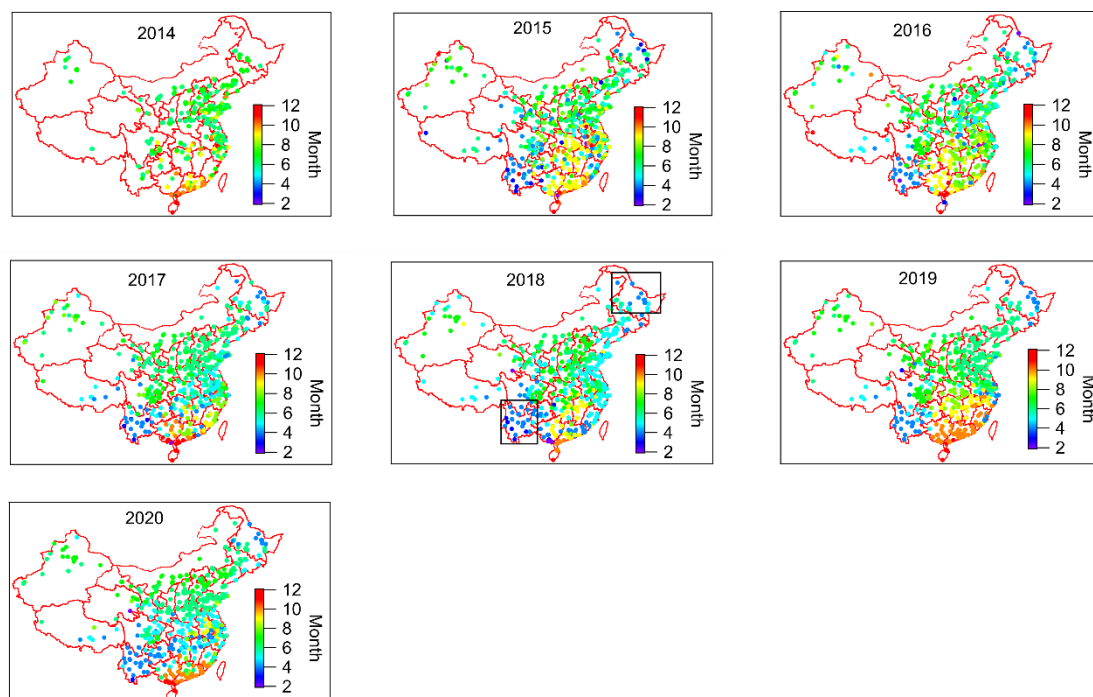
Figure 2. Spatial distribution of the month in which 3MMDA1 ozone concentration occurred during 2014-2020. Rectangles included in the 2018 map in the northeast and southwest China represents the Heilongjiang and Yunnan provinces, respectively.

567

570
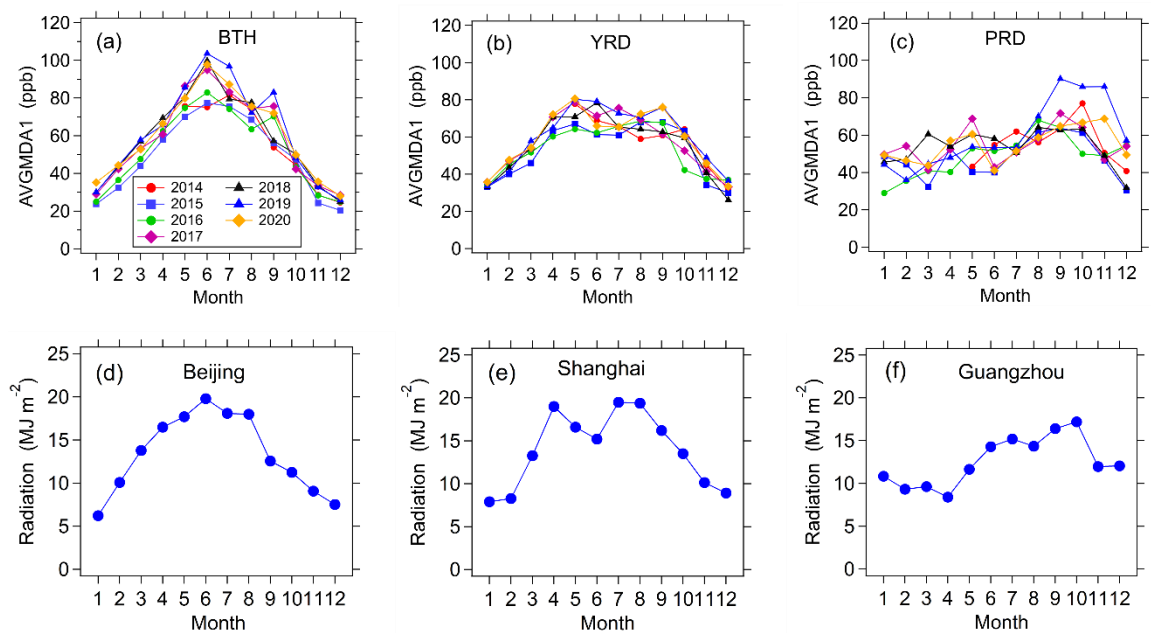
Figure 3. (a), (b) (c): Seasonal variations in monthly mean MDA1 ozone concentrations over all sites in BTH, YRD and PRD during 2014-2020. (d), (e), (f): Seasonal variations in monthly mean solar radiation in representative cities of the three city clusters (Beijing in BTH, Shanghai in YRD and Guangzhou in PRD) in 2013.

576
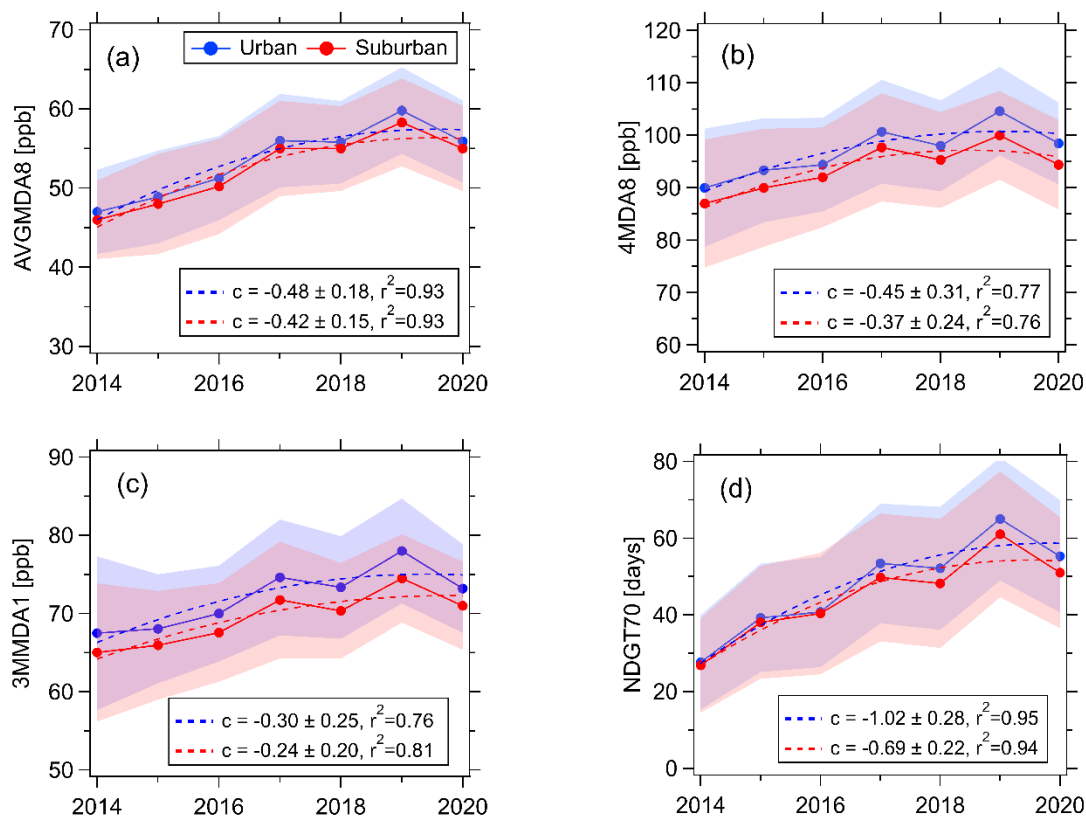
Figure 4. Variations in four ozone metrics (AVGMDA8, 4MDA8, 3MMDA1 and NDGT70) at urban and non-urban sites during 2014-2020. AVGMDA8 is the mean MDA8 $O_3$ in the warm season (April to September), and the other metrics are annual values. Shaded areas represent the range of mean values ± the 50% standard deviation for each metric. The dashed lines are fitted by the polynomial function ($y=a+bx+cx^2$). The quadratic polynomial coefficient c (± one standard deviation) and the determination coefficient $r^2$ are given.

588

589

590
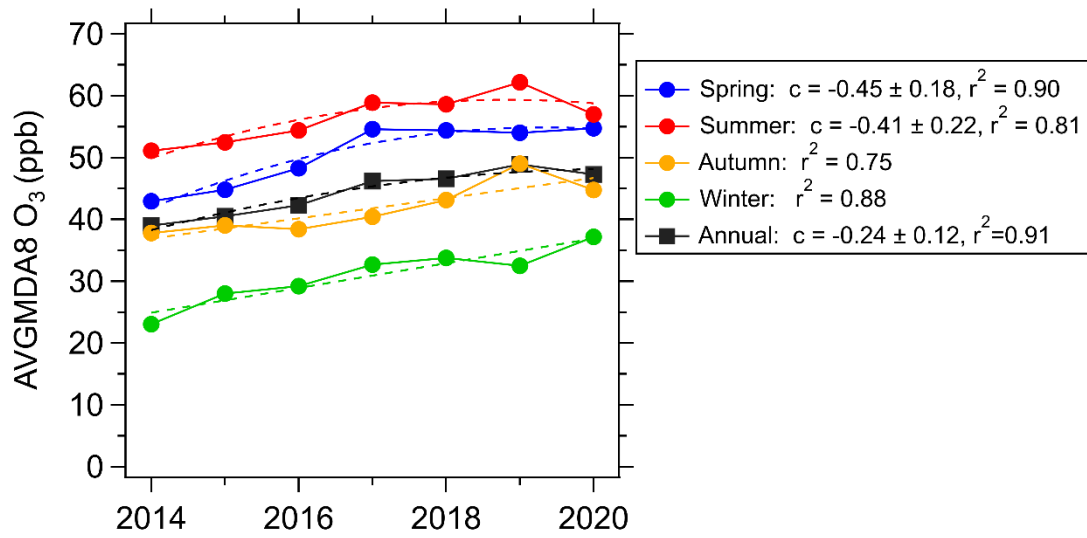
591 Figure 5. Variations in seasonal and annual AVGMDA8 $O_3$ levels during 2014–2020.
592 The trends for spring, summer and annual averages are fitted by the polynomial
593 function (y=a+bx+cx$^2$) and the trends for autumn and winter are fitted by the linear
594 function (y=a+bx). The quadratic polynomial coefficient c (± one standard deviation)
595 and the determination coefficient r$^2$ are given.
596

597

598
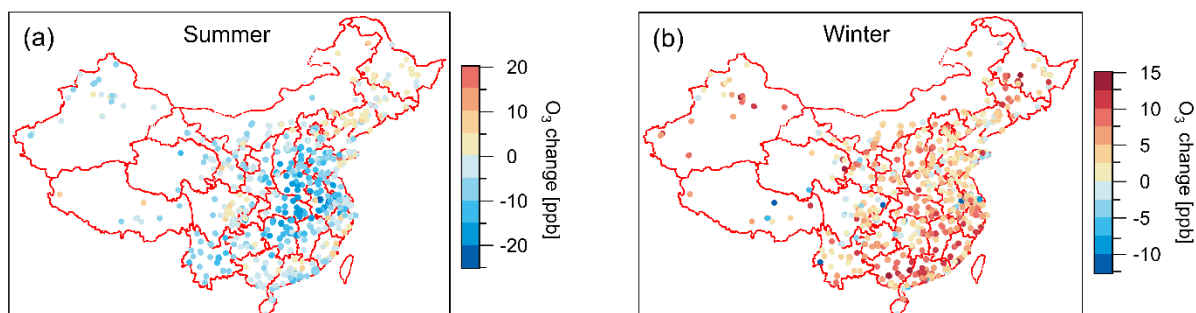
600

601  Figure 6. The change in seasonal averages of MDA8 O$_3$ from 2019 to 2020 in summer
602  (a) and winter (b), China.

603
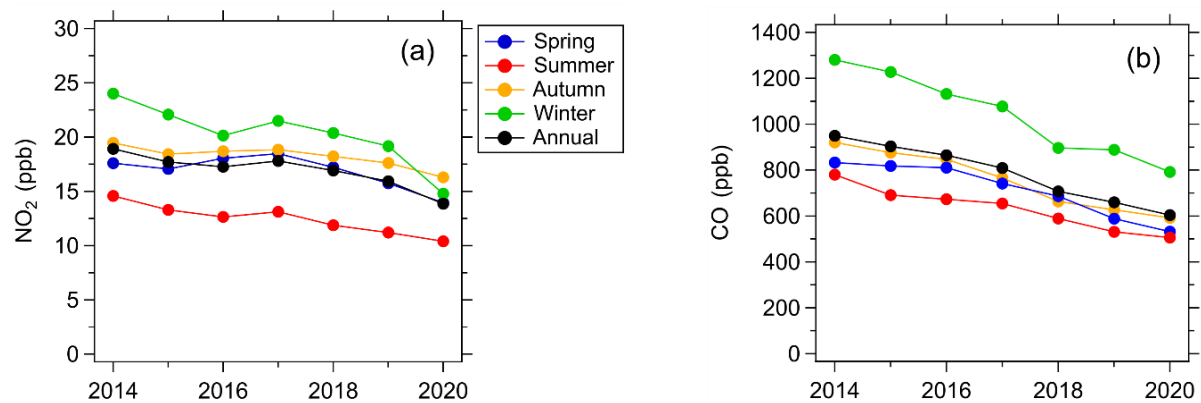
606 Figure 7. Variations in seasonal and annual average concentrations of $NO_2$ and CO
607 measured during 2014–2020 in China.

608
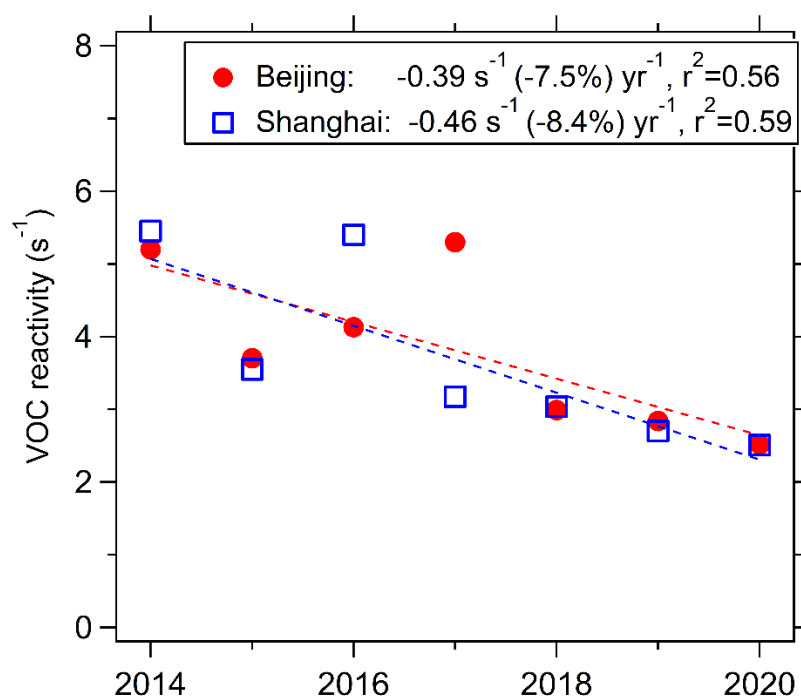
Figure 8. Variations in averages of daytime VOCs reactivity in Beijing and Shanghai, summertime during 2014-2020.

621
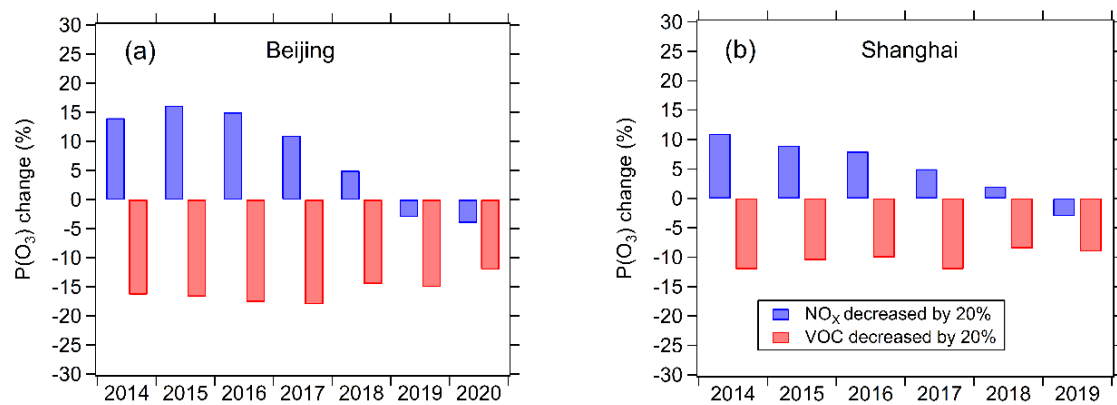
Figure 89. Sensitivity of summertime mean daytime net ozone production rate [P(O$_3$)] to VOCs and NO$_X$ simulated by the photochemical box model during 2014–2020 in Beijing (a) and Shanghai (b). VOCs and NO$_X$ are decreased by 20% to test the fractional change of P(O$_3$).

626

627

628
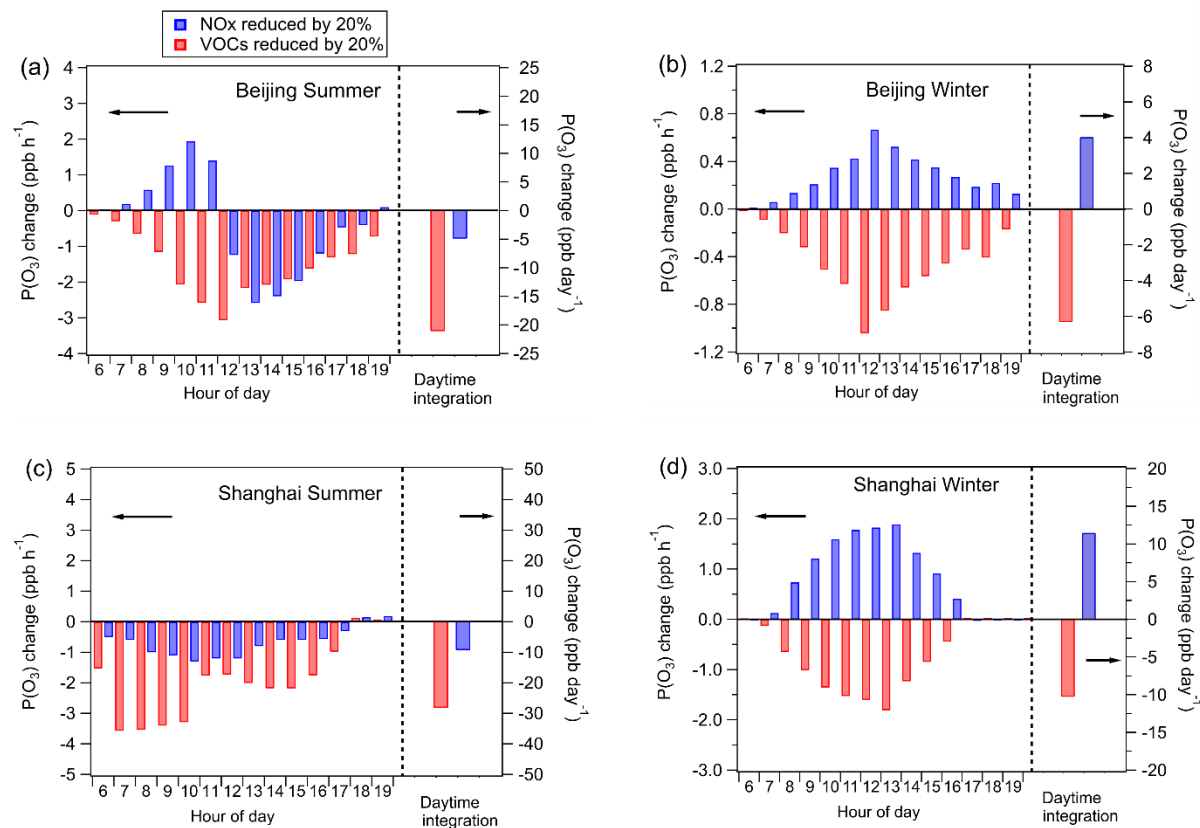
Figure 910. Sensitivity of net ozone production rate [P(O₃)] to 20% reductions in VOCs and NOₓ emissions for summer and winter 2019 in Beijing and Shanghai.

631

632

633 **Table 21.  The reported trends of ozone concentration in China.**

| Spatial scale | Region | Period | Metrics | Ozone trend | References |
|---|---|---|---|---|---|
| Regional scale | Eastern China | 2005–2010 | average ozone column | + 0.23 DU (+1.1%) yr$^{-1}$ | Verstraeten et al. (2015) |
| | North China Plain | 1979–2005 | average tropospheric ozone residual | +1.1 DU (~+3%) decade$^{-1}$ | Xu and Lin (2011) |
| Urban areas | Beijing | 2006–2016 | MDA8 | +2.6 ppb (+3.3%) yr$^{-1}$ | Wang et al. (2020) |
| | Beijing | 1995–2005 | daytime average | +1.0 ppb (+2.0%) yr$^{-1}$ | Ding et al. (2008) |
| | Beijing | 2001–2006 | daily average | +1.1 ppb (+4.1%) yr$^{-1}$ | Tang et al. (2009) |
| | Beijing | 2002–2010 | average ozone column | +1.6 DU (+3.1 %) yr$^{-1}$ | Wang et al. (2012) |
| | Beijing | 2004–2015 | MDA8 | +1.14 ppb (+2.9%) yr$^{-1}$ | Cheng et al. (2016) |
| | Shanghai | 2006–2016 | daily average | +1.1 ppb (+6.7%) yr$^{-1}$ | Gao et al. (2017) |
| | Hong Kong | 1994–2007 | daytime average | +0.58 ppb (+2.0%) yr$^{-1}$ | Wang et al. (2009) |
| | Pearl River Delta | 2006–2019 | 95th percentile | +0.71 ppb (+1.3%) yr$^{-1}$ | Li et al. (2022) |
| | Sichuan Province | 2013–2020 | MDA8 | +2.0 ppb (+4.8%) yr$^{-1}$ | Chen et al. (2021b) |
| | Chinese urban sites | 2013–2019 | MDA8 | +2.4 ppb (+5%) yr$^{-1}$ | Lu et al. (2020) |
| Rural sites | Shangdianzi | 2004–2016 | daytime average | +0.67 ppb (+1.6%) yr$^{-1}$ | Ma et al. (2016); Xu et al. (2020) |
| | Waliguan | 1994–2016 | daytime average | +0.21 ppb (+0.44%) yr$^{-1}$ | Xu et al. (2020) |
| | Akedala | 2009–2016 | daytime average | -1.3 ppb (-3.3%) yr$^{-1}$ | Xu et al. (2020) |
| | Longfengshan | 2005–2016 | daytime average | No trend | Xu et al. (2020) |
| | Lin'an | 2005–2016 | daytime average | No trend | Xu et al. (2020) |
| | Xianggelila | 2007–2016 | daytime average | No trend | Xu et al. (2020) |
| | Changdao | 2013–2019 | MDA8 | No trend | Wang et al. (2020) |

634

635

**Table ~~1~~2. Description of ozone metrics used in this study.**

| Metric | Definition |
|---|---|
| MDA8 (ppb) | daily maximum 8 h average, AVGMDA8 represents mean MDA8 $O_3$ in the focused period. |
| MDA1 (ppb) | daily maximum 1 h average; AVGMDA1 represents mean MDA1 in the focused period |
| 4MDA8 (ppb) | The annual 4th highest MDA8 $O_3$. |
| NDGT70 (days) | The annual total number of days with MDA8 $O_3$ >70 ppb. |
| 3MMDA1 | The annual maximum of the 3-month running mean of the daily maximum 1-hour ozone value. This metric has been used to quantify mortality attributable to long-term ozone exposure. The month in which the 3MMDA1 ozone concentration occurred is the middle month in the 3 months of 3MMDA1. |

637

638

639

640

641

642

643

644

645

646

647

648

649

650

651

652

## References:

China Statistical Yearbook in 2018, Available at http://www.stats.gov.cn/tjsj/ndsj/2018/indexeh.htm, 45, 1817-1829, China Statistics Press, 2018.

Ainsworth, E. A., Yendrek, C. R., Sitch, S., Collins, W. J., and Emberson, L. D.: The effects of tropospheric ozone on net primary productivity and implications for climate change, Annu. Rev. Plant Biol., 63, 637-661, 2012.

Brown-Steiner, B., and Hess, P.: Asian influence on surface ozone in the United States: A comparison of chemistry, seasonality, and transport mechanisms, J. Geophys. Res.-Atmos., 116, 2011.

Chen, X., Jiang, Z., Shen, Y., Li, R., Fu, Y., Liu, J., Han, H., Liao, H., Cheng, X., and Jones, D. B.: Chinese regulations are working—why is surface ozone over industrialized areas still high? Applying lessons from northeast US air quality evolution, Geophys. Res. Lett., 48, e2021GL092816, 2021a.

Chen, Y., Han, H., Zhang, M., Zhao, Y., Huang, Y., Zhou, M., Wang, C., He, G., Huang, R., and Luo, B.: Trends and Variability of Ozone Pollution over the Mountain-Basin Areas in Sichuan Province during 2013–2020: Synoptic Impacts and Formation Regimes, Atmosphere, 12, 1557, 2021b.

Cheng, J., Su, J., Cui, T., Li, X., Dong, X., Sun, F., Yang, Y., Tong, D., Zheng, Y., Li, Y., Li, J., Zhang, Q., and He, K.: Dominant role of emission reduction in PM2.5 air quality improvement in Beijing during 2013–2017: a model-based decomposition analysis, Atmos. Chem. Phys., 19, 6125-6146, 10.5194/acp-19-6125-2019, 2019.

Cheng, N., Li, Y., Zhang, D., Chen, T., Sun, F., Chen, C., and Meng, F.: Characteristics of ground ozone concentration over Beijing from 2004 to 2015: Trends, transport, and effects of reductions, Atmos. Chem. Phys, 2016.

Cooper, O. R., Parrish, D., Stohl, A., Trainer, M., Nédélec, P., Thouret, V., Cammas, J.-P., Oltmans, S., Johnson, B., and Tarasick, D.: Increasing springtime ozone mixing ratios in the free troposphere over western North America, Nature, 463, 344-348, 2010.

Cooper, O. R., Gao, R. S., Tarasick, D., Leblanc, T., and Sweeney, C.: Long-term ozone trends at rural ozone monitoring sites across the United States, 1990–2010, J. Geophys. Res.-Atmos., 117, 2012.

Ding, A., Wang, T., Thouret, V., Cammas, J.-P., and Nédélec, P.: Tropospheric ozone climatology over Beijing: analysis of aircraft data from the MOZAIC program, Atmos. Chem. Phys., 8, 1-13, 2008.

Fiore, A. M., Dentener, F., Wild, O., Cuvelier, C., Schultz, M., Hess, P., Textor, C., Schulz, M., Doherty, R., and Horowitz, L.: Multimodel estimates of intercontinental source-receptor relationships for ozone pollution, J. Geophys. Res.-Atmos., 114, 2009.

Fleming, Z. L., Doherty, R. M., Von Schneidemesser, E., Malley, C. S., Cooper, O. R., Pinto, J. P., Colette, A., Xu, X., Simpson, D., and Schultz, M. G.: Tropospheric Ozone Assessment Report: Present-day ozone distribution and trends relevant to human health, Elem. Sci. Anth., 6, 12, 2018.

Gao, W., Tie, X. X., Xu, J. M., Huang, R. J., Mao, X. Q., Zhou, G. Q., and Chang, L. Y.: Long-term trend of O-3 in a mega City (Shanghai), China: Characteristics, causes, and interactions with precursors, Sci. Total Environ., 603, 425-433, 10.1016/j.scitotenv.2017.06.099, 2017.

Gaudel, A., Cooper, O. R., Chang, K.-L., Bourgeois, I., Ziemke, J. R., Strode, S. A., Oman, L. D., Sellitto, P., Nédélec, P., and Blot, R.: Aircraft observations since the 1990s reveal increases of

696   tropospheric ozone at multiple locations across the Northern Hemisphere, Sci. Adv., 6, eaba8272,
697   2020.

698   Han, X., Zhu, L., Wang, S., Meng, X., Zhang, M., and Hu, J.: Modeling study of impacts on surface
699   ozone of regional transport and emissions reductions over North China Plain in summer 2015,
700   Atmos. Chem. Phys., 18, 12207-12221, 2018.

701   He, J., Gong, S., Yu, Y., Yu, L., Wu, L., Mao, H., Song, C., Zhao, S., Liu, H., and Li, X.: Air pollution
702   characteristics and their relation to meteorological conditions during 2014–2015 in major
703   Chinese cities, Environmental pollution, 223, 484-496, 2017.

704   Hendrick, F., Müller, J.-F., Clémer, K., Wang, P., De Mazière, M., Fayt, C., Gielen, C., Hermans, C.,
705   Ma, J., and Pinardi, G.: Four years of ground-based MAX-DOAS observations of HONO and NO
706   2 in the Beijing area, Atmos. Chem. Phys., 14, 765-781, 2014.

707   Jacob, D. J., and Winner, D. A.: Effect of climate change on air quality, Atmos. Environ., 43, 51-63,
708   2009.

709   Jiang, H., Lu, N., Qin, J., and Yao, L.: Surface global and diffuse solar radiation over China
710   acquired from geostationary Multi-functional Transport Satellite data, Earth System Science Data
711   Discussions, 1-22, 2019.

712   Jindal, S.: Air quality guidelines: Global update 2005, Particulate matter, ozone, nitrogen dioxide
713   and sulfur dioxide, Indian J. Med. Res., 126, 492-494, 2007.

714   Kang, M., Zhang, J., Zhang, H., and Ying, Q.: On the Relevancy of Observed Ozone Increase
715   during COVID-19 Lockdown to Summertime Ozone and PM2.5 Control Policies in China, Environ.
716   Sci. Technol. Lett., 8, 289-294, 2021.

717   Kleinman, L. I.: Low and high NOx tropospheric photochemistry, J. Geophys. Res.-Atmos., 99,
718   16831-16838, 1994.

719   Kleinman, L. I., Daum, P. H., Lee, J. H., Lee, Y. N., Nunnermacker, L. J., Springston, S. R., Newman,
720   L., Weinstein‐Lloyd, J., and Sillman, S.: Dependence of ozone production on NO and
721   hydrocarbons in the troposphere, Geophys. Res. Lett., 24, 2299-2302, 1997.

722   Kleinman, L. I.: The dependence of tropospheric ozone production rate on ozone precursors,
723   Atmos. Environ., 39, 575-586, https://doi.org/10.1016/j.atmosenv.2004.08.047, 2005.

724   Le, T., Wang, Y., Liu, L., Yang, J., Yung, Y. L., Li, G., and Seinfeld, J. H.: Unexpected air pollution
725   with marked emission reductions during the COVID-19 outbreak in China, Science, 369, 702-706,
726   2020.

727   Lefohn, A. S., Malley, C. S., Smith, L., Wells, B., Hazucha, M., Simon, H., Naik, V., Mills, G., Schultz,
728   M. G., and Paoletti, E.: Tropospheric ozone assessment report: Global ozone metrics for climate
729   change, human health, and crop/ecosystem research, Elem. Sci. Anth., 6, 2018.

730   Li, J., Lu, K., Lv, W., Li, J., Zhong, L., Ou, Y., Chen, D., Huang, X., and Zhang, Y.: Fast increasing of
731   surface ozone concentrations in Pearl River Delta characterized by a regional air quality
732   monitoring network during 2006–2011, J. Environ. Sci., 26, 23-36, 2014.

733   Li, K., Jacob, D. J., Liao, H., Shen, L., Zhang, Q., and Bates, K. H.: Anthropogenic drivers of 2013–
734   2017 trends in summer surface ozone in China, Proc. National Acad. Sci., 116, 422-427, 2019a.

735   Li, K., Jacob, D. J., Shen, L., Lu, X., De Smedt, I., and Liao, H.: Increases in surface ozone pollution
736   in China from 2013 to 2019: anthropogenic and meteorological influences, Atmos. Chem. Phys.,
737   20, 11423-11433, 2020.

738   Li, K., Jacob, D. J., Liao, H., Qiu, Y., Shen, L., Zhai, S., Bates, K. H., Sulprizio, M. P., Song, S., and Lu,
739   X.: Ozone pollution in the North China Plain spreading into the late-winter haze season, Proc.

740 National Acad. Sci., 118, 2021.

741 Li, M., Zhang, Q., Zheng, B., Tong, D., Lei, Y., Liu, F., Hong, C., Kang, S., Yan, L., and Zhang, Y.:
742 Persistent growth of anthropogenic non-methane volatile organic compound (NMVOC)
743 emissions in China during 1990–2017: drivers, speciation and ozone formation potential, Atmos.
744 Chem. Phys., 19, 8897-8913, 2019b.

745 Li, X.-B., Yuan, B., Parrish, D. D., Chen, D., Song, Y., Yang, S., Liu, Z., and Shao, M.: Long-term
746 trend of ozone in southern China reveals future mitigation strategy for air pollution, Atmos.
747 Environ., 269, 118869, 2022.

748 Lin, M., Fiore, A. M., Horowitz, L. W., Cooper, O. R., Naik, V., Holloway, J., Johnson, B. J.,
749 Middlebrook, A. M., Oltmans, S. J., and Pollack, I. B.: Transport of Asian ozone pollution into
750 surface air over the western United States in spring, J. Geophys. Res.-Atmos., 117, 2012.

751 Liu, F., Zhang, Q., Zheng, B., Tong, D., Yan, L., Zheng, Y., and He, K.: Recent reduction in NO x
752 emissions over China: synthesis of satellite observations and emission inventories, Environ. Res.
753 Lett., 11, 114002, 2016.

754 Liu, H., Liu, S., Xue, B., Lv, Z., Meng, Z., Yang, X., Xue, T., Yu, Q., and He, K.: Ground-level ozone
755 pollution and its health impacts in China, Atmos. Environ., 173, 223-230, 2018.

756 Lu, X., Hong, J. Y., Zhang, L., Cooper, O. R., Schultz, M. G., Xu, X. B., Wang, T., Gao, M., Zhao, Y. H.,
757 and Zhang, Y. H.: Severe Surface Ozone Pollution in China: A Global Perspective, Environ. Sci.
758 Technol. Lett., 5, 487-494, 10.1021/acs.estlett.8b00366, 2018.

759 Lu, X., Zhang, L., Wang, X., Gao, M., Li, K., Zhang, Y., Yue, X., and Zhang, Y.: Rapid increases in
760 warm-season surface ozone and resulting health impact in China since 2013, Environ. Sci.
761 Technol. Lett., 7, 240-247, 2020.

762 Ma, Z. Q., Xu, J., Quan, W. J., Zhang, Z. Y., Lin, W. L., and Xu, X. B.: Significant increase of surface
763 ozone at a rural site, north of eastern China, Atmos. Chem. Phys., 16, 3969-3977, 10.5194/acp-
764 16-3969-2016, 2016.

765 Malley, C. S., Henze, D. K., Kuylenstierna, J. C., Vallack, H. W., Davila, Y., Anenberg, S. C., Turner,
766 M. C., and Ashmore, M. R.: Updated global estimates of respiratory mortality in adults ≥ 30 years
767 of age attributable to long-term ozone exposure, Environ. Health Perspect., 125, 087021, 2017.

768 Mihelcic, D., Holland, F., Hofzumahaus, A., Hoppe, L., Konrad, S., Müsgen, P., Pätz, H. W., Schäfer,
769 H. J., Schmitz, T., and Volz-Thomas, A.: Peroxy radicals during BERLIOZ at Pabstthum:
770 Measurements, radical budgets and ozone production, J. Geophys. Res.-Atmos., 108, 2003.

771 Mills, G., Pleijel, H., Malley, C. S., Sinha, B., Cooper, O. R., Schultz, M. G., Neufeld, H. S., Simpson,
772 D., Sharps, K., and Feng, Z.: Tropospheric Ozone Assessment Report: Present-day tropospheric
773 ozone distribution and trends relevant to vegetation, Elem. Sci. Anth., 6, 2018.

774 Monks, P. S., Archibald, A., Colette, A., Cooper, O., Coyle, M., Derwent, R., Fowler, D., Granier, C.,
775 Law, K. S., and Mills, G.: Tropospheric ozone and its precursors from the urban to the global scale
776 from air quality to short-lived climate forcer, Atmos. Chem. Phys., 15, 8889-8973, 2015.

777 Parrish, D. D., Derwent, R. G., Steinbrecht, W., Stübi, R., Van Malderen, R., Steinbacher, M., Trickl,
778 T., Ries, L., and Xu, X.: Zonal similarity of long-term changes and seasonal cycles of baseline
779 ozone at northern midlatitudes, J. Geophys. Res.-Atmos., 125, e2019JD031908, 2020.

780 Qu, K., Wang, X., Yan, Y., Shen, J., Xiao, T., Dong, H., Zeng, L., and Zhang, Y.: A comparative study
781 to reveal the influence of typhoons on the transport, production and accumulation of O3 in the
782 Pearl River Delta, China, Atmos. Chem. Phys., 21, 11593-11612, 2021.

783 Shah, V., Jacob, D. J., Li, K., Silvern, R. F., Zhai, S. X., Liu, M. Y., Lin, J. T., and Zhang, Q.: Effect of

changing NOx lifetime on the seasonality and long-term trends of satellite-observed tropospheric NO2 columns over China, Atmos. Chem. Phys., 20, 1483-1495, 10.5194/acp-20-1483-2020, 2020.

Shao, M., Wang, W., Yuan, B., Parrish, D. D., Li, X., Lu, K., Wu, L., Wang, X., Mo, Z., and Yang, S.: Quantifying the role of PM2. 5 dropping in variations of ground-level ozone: Inter-comparison between Beijing and Los Angeles, Sci. Total Environ., 147712, 2021.

Shen, L., Liu, J., Zhao, T., Xu, X., Han, H., Wang, H., and Shu, Z.: Atmospheric transport drives regional interactions of ozone pollution in China, Sci. Total Environ., 830, 154634, 2022.

Stevenson, D., Dentener, F., Schultz, M., Ellingsen, K., Van Noije, T., Wild, O., Zeng, G., Amann, M., Atherton, C., and Bell, N.: Multimodel ensemble simulations of present-day and near-future tropospheric ozone, J. Geophys. Res.-Atmos., 111, 2006.

Stocker, T. F., Qin, D., Plattner, G.-K., Tignor, M. M., Allen, S. K., Boschung, J., Nauels, A., Xia, Y., Bex, V., and Midgley, P. M.: Climate Change 2013: The physical science basis. contribution of working group I to the fifth assessment report of IPCC the intergovernmental panel on climate change, 2014.

Stohl, A., Bonasoni, P., Cristofanelli, P., Collins, W., Feichter, J., Frank, A., Forster, C., Gerasopoulos, E., Gäggeler, H., and James, P.: Stratosphere-troposphere exchange: A review, and what we have learned from STACCATO, J. Geophys. Res.-Atmos., 108, 2003.

Sun, J., Wang, Y., Wu, F., Tang, G., Wang, L., Wang, Y., and Yang, Y.: Vertical characteristics of VOCs in the lower troposphere over the North China Plain during pollution periods, Environmental Pollution, 236, 907-915, 2018.

Sun, L., Xue, L., Wang, T., Gao, J., Ding, A., Cooper, O. R., Lin, M., Xu, P., Wang, Z., and Wang, X.: Significant increase of summertime ozone at Mount Tai in Central Eastern China, Atmos. Chem. Phys., 16, 10637-10650, 2016.

Tang, G., Li, X., Wang, Y., Xin, J., and Ren, X.: Surface ozone trend details and interpretations in Beijing, 2001–2006, Atmos. Chem. Phys., 9, 8813-8823, 2009.

Tang, G., Liu, Y., Zhang, J., Liu, B., Li, Q., Sun, J., Wang, Y., Xuan, Y., Li, Y., and Pan, J.: Bypassing the NOx titration trap in ozone pollution control in Beijing, Atmos. Res., 249, 105333, 2021.

Trickl, T., Bärtsch-Ritter, N., Eisele, H., Furger, M., Mücke, R., Sprenger, M., and Stohl, A.: High-ozone layers in the middle and upper troposphere above Central Europe: potential import from the stratosphere along the subtropical jet stream, Atmos. Chem. Phys., 11, 9343-9366, 2011.

Verstraeten, W. W., Neu, J. L., Williams, J. E., Bowman, K. W., Worden, J. R., and Boersma, K. F.: Rapid increases in tropospheric ozone production and export from China, Nat. Geosci., 8, 690-+, 10.1038/ngeo2493, 2015.

Wang, B., Shao, M., Lu, S. H., Yuan, B., Zhao, Y., Wang, M., Zhang, S. Q., and Wu, D.: Variation of ambient non-methane hydrocarbons in Beijing city in summer 2008, Atmos. Chem. Phys., 10, 5911-5923, 10.5194/acp-10-5911-2010, 2010.

Wang, M., Zeng, L., Lu, S., Shao, M., Liu, X., Yu, X., Chen, W., Yuan, B., Zhang, Q., and Hu, M.: Development and validation of a cryogen-free automatic gas chromatograph system (GC-MS/FID) for online measurements of volatile organic compounds, Anal. Methods, 6, 9424-9434, 2014.

Wang, P., Yang, Y., Li, H., Chen, L., Dang, R., Xue, D., Li, B., Tang, J., Leung, L. R., and Liao, H.: North China Plain as a hot spot of ozone pollution exacerbated by extreme high temperatures, Atmospheric Chemistry and Physics Discussions, 1-35, 2021a.

Wang, T., Wei, X., Ding, A., Poon, C., Lam, K. S., Li, Y. S., Chan, L., and Anson, M.: Increasing surface ozone concentrations in the background atmosphere of Southern China, 1994–2007, Atmos. Chem. Phys., 9, 6217-6227, 2009.

Wang, W., Li, X., Shao, M., Hu, M., Zeng, L., Wu, Y., and Tan, T.: The impact of aerosols on photolysis frequencies and ozone production in Beijing during the 4-year period 2012–2015, Atmos. Chem. Phys., 19, 9413-9429, 10.5194/acp-19-9413-2019, 2019.

Wang, W., Parrish, D. D., Li, X., Shao, M., Liu, Y., Mo, Z., Lu, S., Hu, M., Fang, X., and Wu, Y.: Exploring the drivers of the increased ozone production in Beijing in summertime during 2005–2016, Atmos. Chem. Phys., 20, 15617-15633, 2020.

Wang, W., Li, X., Kuang, Y., Su, H., Cheng, Y., Hu, M., Zeng, L., Tan, T., and Zhang, Y.: Exploring the Drivers and Photochemical Impact of the Positive Correlation between Single Scattering Albedo and Aerosol Optical Depth in the Troposphere, Environ. Sci. Technol. Lett., 2021b.

Wang, W., Qi, J., Zhou, J., Yuan, B., Peng, Y., Wang, S., Yang, S., Williams, J., Sinha, V., and Shao, M.: The improved comparative reactivity method (ICRM): measurements of OH reactivity under high-NO x conditions in ambient air, Atmos. Meas. Tech., 14, 2285-2298, 2021c.

Wang, W., van der A, R., Ding, J., van Weele, M., and Cheng, T.: Spatial and temporal changes of the ozone sensitivity in China based on satellite and ground-based observations, Atmos. Chem. Phys., 21, 7253-7269, 10.5194/acp-21-7253-2021, 2021d.

Wang, Y., Konopka, P., Liu, Y., Chen, H., Müller, R., Plöger, F., Riese, M., Cai, Z., and Lü, D.: Tropospheric ozone trend over Beijing from 2002–2010: ozonesonde measurements and modeling analysis, Atmos. Chem. Phys., 12, 8389-8399, 2012.

Xiao, Z., and Jiang, H.: A study of spatial and temporal dynamics of total ozone over Southwest China with multi-source remote-sensing data, Int. J. Remote Sens., 34, 128-138, 2013.

Xu, J., Ma, J. Z., Zhang, X. L., Xu, X. B., Xu, X. F., Lin, W. L., Wang, Y., Meng, W., and Ma, Z. Q.: Measurements of ozone and its precursors in Beijing during summertime: impact of urban plumes on ozone pollution in downwind rural areas, Atmos. Chem. Phys., 11, 12241-12252, 10.5194/acp-11-12241-2011, 2011.

Xu, J., Tie, X., Gao, W., Lin, Y., and Fu, Q.: Measurement and model analyses of the ozone variation during 2006 to 2015 and its response to emission change in megacity Shanghai, China, Atmos. Chem. Phys., 19, 9017-9035, 10.5194/acp-19-9017-2019, 2019.

Xu, W., Xu, X., Lin, M., Lin, W., Tarasick, D., Tang, J., Ma, J., and Zheng, X.: Long-term trends of surface ozone and its influencing factors at the Mt Waliguan GAW station, China – Part 2: The roles of anthropogenic emissions and climate variability, Atmos. Chem. Phys., 18, 773-798, 10.5194/acp-18-773-2018, 2018.

Xu, X., and Lin, W.: Trends of tropospheric ozone over China based on satellite data (1979–2005), Adv. Clim. Chang. Res., 2, 43-48, 2011.

Xu, X., Lin, W., Xu, W., Jin, J., Wang, Y., Zhang, G., Zhang, X., Ma, Z., Dong, Y., and Ma, Q.: Long-term changes of regional ozone in China: implications for human health and ecosystem impacts, Elem. Sci. Anth., 8, 2020.

Yang, Y., Li, M., Wang, H., Li, H., Wang, P., Li, K., Gao, M., and Liao, H.: ENSO modulation of summertime tropospheric ozone over China, Environ. Res. Lett., 17, 034020, 2022.

Yin, C., Solmon, F., Deng, X., Zou, Y., Deng, T., Wang, N., Li, F., Mai, B., and Liu, L.: Geographical distribution of ozone seasonality over China, Sci. Total Environ., 689, 625-633, 2019.

Young, P., Archibald, A., Bowman, K., Lamarque, J.-F., Naik, V., Stevenson, D., Tilmes, S.,

872    Voulgarakis, A., Wild, O., and Bergmann, D.: Pre-industrial to end 21st century projections of

873    tropospheric ozone from the Atmospheric Chemistry and Climate Model Intercomparison

874    Project (ACCMIP), Atmos. Chem. Phys., 13, 2063-2090, 2013.

875    Zhang, J. P., Zhu, T., Zhang, Q. H., Li, C. C., Shu, H. L., Ying, Y., Dai, Z. P., Wang, X., Liu, X. Y., Liang,

876    A. M., Shen, H. X., and Yi, B. Q.: The impact of circulation patterns on regional transport pathways

877    and air quality over Beijing and its surroundings, Atmos. Chem. Phys., 12, 5031-5053,

878    10.5194/acp-12-5031-2012, 2012.

879    Zhang, K., Xiu, G., Zhou, L., Bian, Q., Duan, Y., Fei, D., Wang, D., and Fu, Q.: Vertical distribution of

880    volatile organic compounds within the lower troposphere in late spring of Shanghai, Atmos.

881    Environ., 186, 150-157, 2018.

882    Zhang, Q., Yuan, B., Shao, M., Wang, X., Lu, S., Lu, K., Wang, M., Chen, L., Chang, C.-C., and Liu, S.:

883    Variations of ground-level O3 and its precursors in Beijing in summertime between 2005 and

884    2011, Atmos. Chem. Phys., 14, 6089-6101, 2014.

885    Zheng, B., Zhang, Q., Geng, G., Chen, C., Shi, Q., Cui, M., Lei, Y., and He, K.: Changes in China's

886    anthropogenic emissions and air quality during the COVID-19 pandemic in 2020, Earth Syst. Sci.

887    Data, 13, 2895-2907, 10.5194/essd-13-2895-2021, 2021.

888

889

890

892
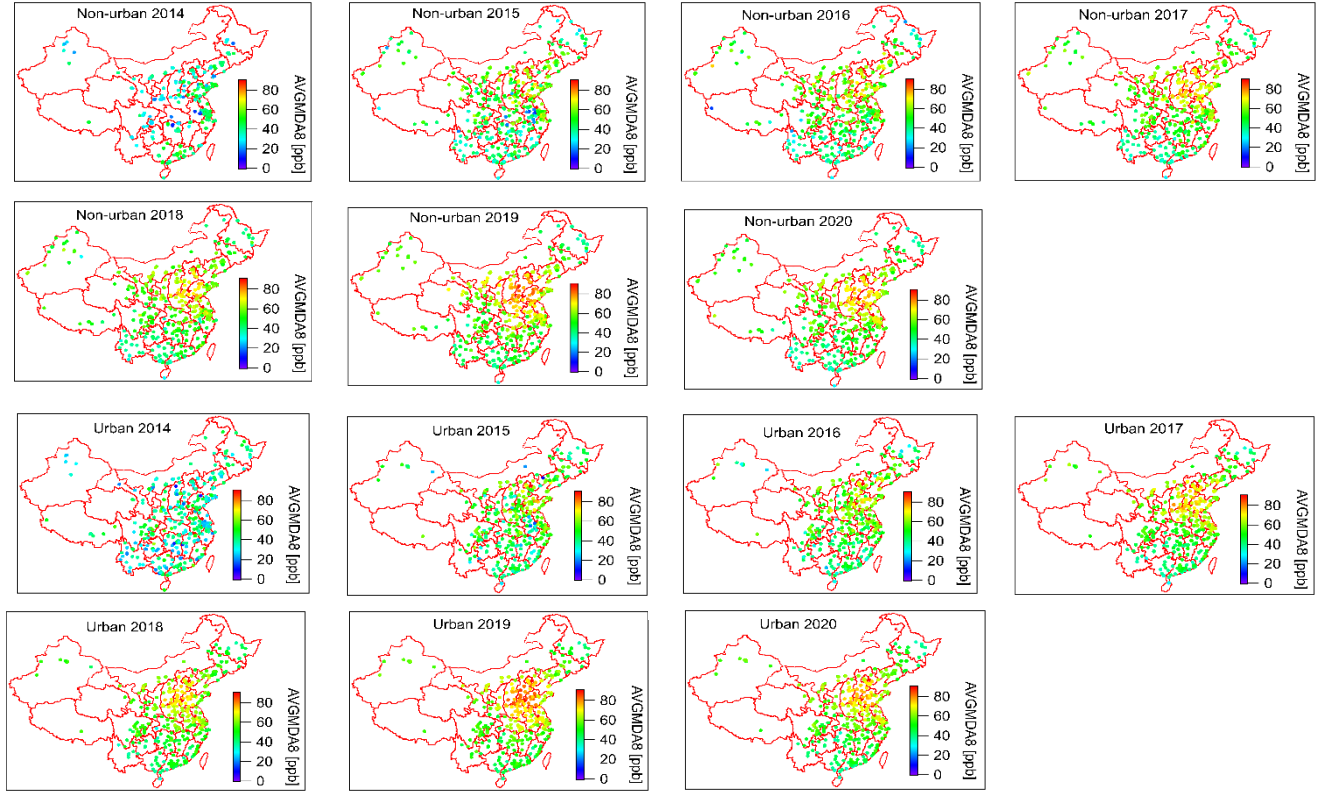
Figure S1. Spatial distribution of warm-season AVGMDA8 ozone concentrations in urban and non urban areas during 2014 2020.

909

910

911

912

913

914

915

916

917

918